Composites Science and Technology 247 (2024) 110398

Contents lists available at ScienceDirect

Composites Science and Technology

journal homepage: www.elsevier.com/locate/compscitech

Preparation of superhydrophobic shape memory composites with uniform wettability and morphing performance

Xinlin Li [a], Bin Zhan [b], Xueting Wang [c], Yan Liu [b], Yanju Liu [c,*], Jinsong Leng [a,**]

[a] Centre for Composite Materials and Structures, Harbin Institute of Technology (HIT), Harbin, 150080, PR China
[b] Key Laboratory of Bionic Engineering (Ministry of Education), Jilin University, Changchun, 130022, PR China
[c] Department of Astronautical Science and Mechanics, Harbin Institute of Technology (HIT), Harbin, 150080, PR China

ARTICLE INFO

Keywords:
Superhydrophobic
Shape memory effect
Uniform wettability
Shape morphing
Marine deployable structures

ABSTRACT

Superhydrophobic shape memory surfaces have attracted much attention in recent years, as they can intelligently control surface wettability. However, less research has focused on the development of superhydrophobic shape memory materials that can maintain uniform wettability in any morphing shape. It is common in nature that species such as lotus leaves and kingfisher show good superhydrophobicity in any movement under/on water. Based on this inspiration, this work presents a novel superhydrophobic shape memory composite (SSMC) by coupling superhydrophobic coatings and shape memory epoxy composites. The SSMC exhibits excellent water repellency and self-cleaning performance regardless of how it is bent. In addition, its good shape memory effect and variable stiffness characteristics enable it to be potentially used as deployable marine structures and morphing skin of aquatic unmanned aerial vehicles. On the other hand, the SSMC also offers good anti-icing properties and mechanical/chemical robustness that enhance long-term service performance all year round. This research provides a fresh idea for the design of new smart superhydrophobic materials and expands applications in the field of marine and aviation facilities.

1. Introduction

In the past decades, the lotus leaf has been widely studied as a representative prototype with specific hydrophobic and self-cleaning properties. Inspired by the lotus leaf, the superhydrophobic surface is recognized as a good candidate that can be used in various fields such as drag reduction, anti-icing, anti-corrosion, anti-fouling, etc. To achieve superhydrophobicity, micro/nanostructures and low surface energy are two important factors. Recently, research on superhydrophobic materials has mainly focused on two different regimes. One is to keep the stable superhydrophobic performance by maintaining the rough structures and surface chemicals, i.e. impalement resistance [1], mechanical/chemical robustness [2,3], or weather resistance [4]. For example, Wei et al. [5] reported the design of superhydrophobic POA/-fluoroPOS@silica coatings with isotropic three-tier hierarchical structures by a spraying method. The coatings on 5G radomes can not only prevent rain droplet accumulation to inhibit signal loss but also exhibit good weather resistance. Wang et al. [2] presented the concept of an armor structure in the fabrication of a superhydrophobic surface with mechanical robustness that was able to undertake the abrasion of sandpaper and a sharp steel blade. The other strategy is to intelligently control the surface wettability by altering the surface chemical properties [6,7]. Yu et al. [8] achieved a reversible wettability switch between superhydrophilic and superhydrophobic states by changing the adsorption process of oxygen and water using ultraviolet radiation.

In addition, surfaces based on shape memory polymers and composites have been widely studied, which can smartly change the physical situations of microstructures [9,10]. Shape memory polymers (SMPs) are one of the representative smart materials [11–13]. Its shapes can be memorized temporarily and also return to the original (permanent) shapes under external stimuli (such as temperature, light, electricity, magnetic field, and so on) [14–16]. By applying the shape memory effect, the shapes of microstructures on superhydrophobic surfaces can be fixed under external pressure and restored in response to multi-stimuli. Consequently, the wettability of the superhydrophobic surface is deliberately controlled by reshaping the microstructures on demand. Template method and photolithography are two popular strategies to prepare superhydrophobic shape memory micro/nanostructures. Shao

* Corresponding author.
** Corresponding author.
E-mail addresses: yj_liu@hit.edu.cn (Y. Liu), lengjs@hit.edu.cn (J. Leng).

https://doi.org/10.1016/j.compscitech.2023.110398
Received 15 July 2023; Received in revised form 7 October 2023; Accepted 12 December 2023
Available online 20 December 2023

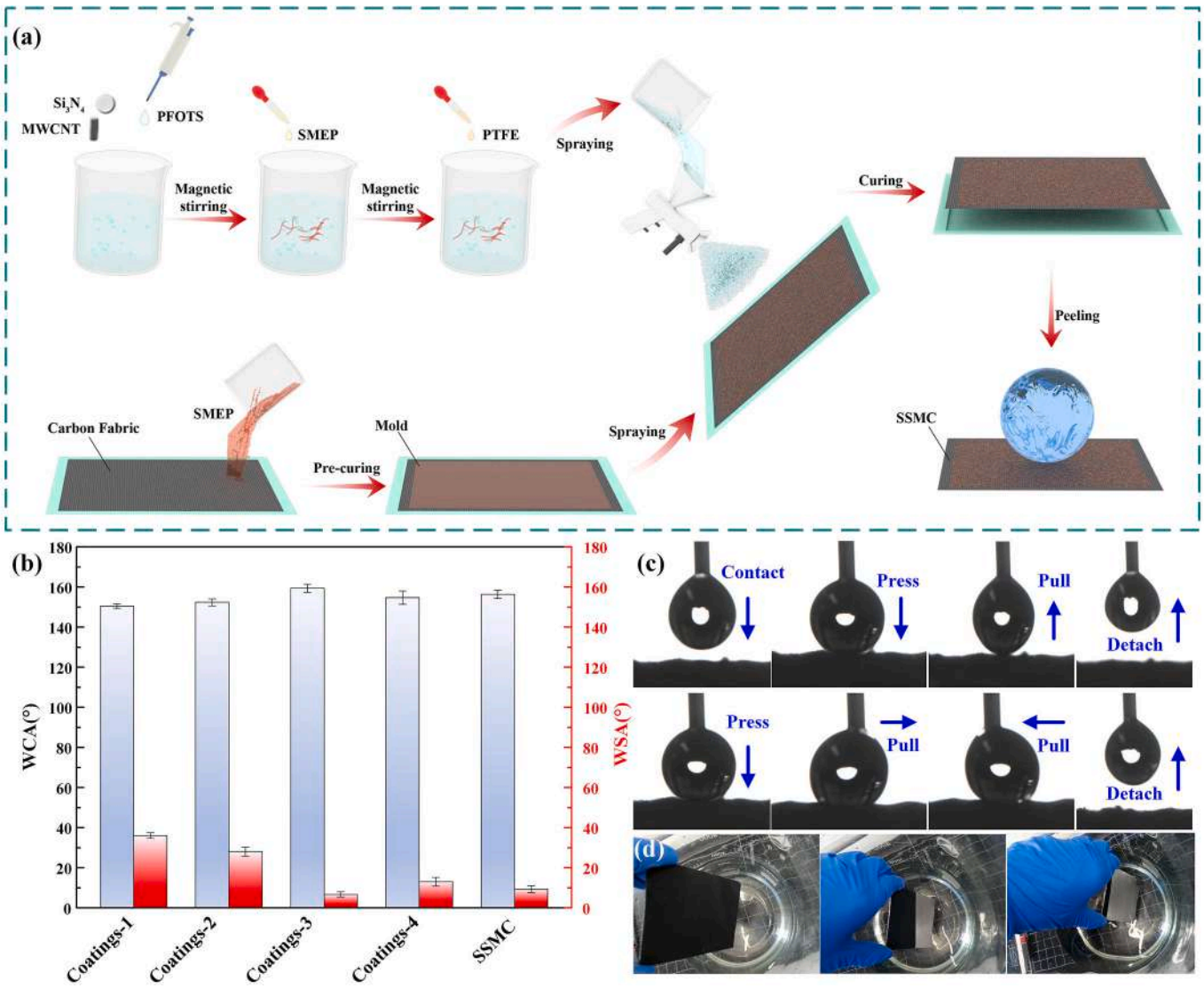

Fig. 1. (a) Schematic of preparation process of SSMC. (b) Wettability of different samples. (c) Liquid repellent performance investigation. (d) Silver mirror effect on SSMC.

et al. [17] fabricated shape memory micro/nanostructure arrays through the template method. The micropillar arrays showed photothermal-responsive performance, leading to a reversible wettability change regulated by near-infrared (NIR) light. Instead of templating microarrays, Bai et al. [18] fabricated shape memory microgrooves by femtosecond laser direct writing. The groove-structured surface showed reversible wettability changes depending on the shape deformation of SMP microgroove arrays. Apart from the aforementioned fabrication method, the fabrication of microstructures is also effective by combining top-down and bottom-up methods [9]. Consequently, the diverse stimuli approaches extend the potential applications of such smart wetting surfaces, such as water transportation [19], soft robotics with tunable adhesion [20], tunable metasurfaces [21], and multifunctional sensors [22]. However, less research has focused on achieving uniform superhydrophobic performance on shape memory substrates.

In addition, SMPs and SMP composites can also be designed and used in macro components based on their controllable active deformation. One of the most important applications is deployable aerospace structures [23–25]. Ming et al. [26] developed a deployable SMP composite parabolic reflector with vacuum-assisted resin infusion technology. The parabolic reflector was fixed in a 6-Pl configuration and deployed automatically when heated over the glass-transition temperature, which provided important experience and data for the design of space telescopes and space antennas. In addition, the advantages of SMPs and SMP composites, such as variable stiffness and light-weight properties, enable them to be potentially used in morphing aircraft [27–30]. Li et al. [31] proposed a direct heating method for SMP morphing skin by fabricating it with conductive elastic fabric, which did not require a heating source. Therefore, SMPs and SMP composites, when functionalized by superhydrophobicity, are expected to have the potential to be widely used in marine installations or unmanned aerial-aquatic vehicles.

In this work, superhydrophobic smart materials with uniform wettability were prepared by spraying superhydrophobic coatings on a pre-cured shape memory epoxy substrate. The as-prepared superhydrophobic shape memory composite (SSMC) provided excellent water repellent and self-cleaning performance like a lotus leaf when immersed in polluted water at different bending shapes. In addition, the SSMC presented a low glass transition temperature and fast recovery time, which dramatically reduced the requirements of the heating system. In this case, the use of deployable marine structures and morphing skin in the coupling of superhydrophobicity and shape memory property was investigated and demonstrated. Meanwhile, the good anti-icing property and mechanical/chemical robustness of SSMC enhance the long-term

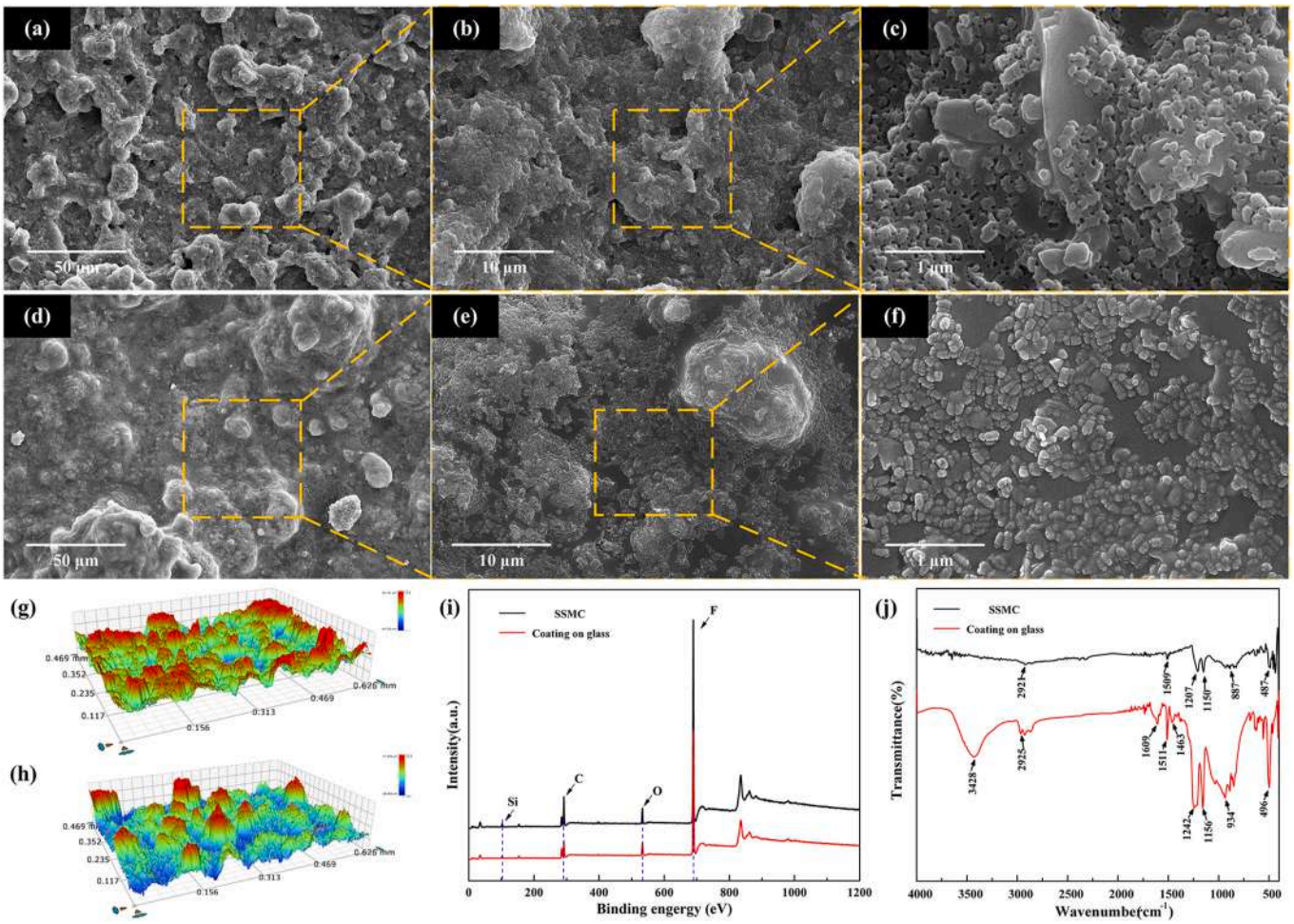

Fig. 2. SEM images of coatings on glass substrate (a, b, c) and on shape memory composite substrates (d, e, f). (g) and (h) are the 3D optical microscope images of coatings on glass substrate and SSMC, respectively. (i) and (j) are the corresponding XPS and FTIR spectra of the coatings on as-prepared substrates, respectively.

service performance all year round. Therefore, this work is hoping to provide new insights into the design of smart superhydrophobic materials for future applications.

2. Experiment

2.1. Materials

Carbon nanotubes (MWNTs) and Bisphenol-a type epoxy resin were purchased from Suzhou Tanfeng Graphene Technology Co., Ltd., and Nantong Xingchen Synthetic Material Co. Ltd, respectively. 1H,1H,2H,2H-perfluorooctyl trichlorosilane (PFOTS) and Polytetrafluoroethylene (PTFE) dispersion were purchased from Macklin Biochemical Technology Co., Ltd. Silicon nitride were purchased from Yuante New Materials Co., Ltd. Shape memory epoxy resin (SMEP) was made by bisphenol-A epoxy resin and Jeffamine D230 in our lab.

2.2. Preparation of superhydrophobic coatings

The preparation process of superhydrophobic shape memory composite (SSMC) is illustrated in Fig. 1a. First, 0.5 g MWNTs and 2 g Si_3N_4 were dispersed in 100 mL of acetone with magnetic stirring at 300 r/min for 5min. Subsequently, 1%wt PFOTS was added to the above solution and magnetically stirred at 300 r/min for 12 h at room temperature. Then, 5 g of shape memory epoxy resin was added in the solution followed by magnetic stirring at 500 r/min for 6 h. In the following procedure, a PTFE dispersion was added with a weight ratio of 1:x (SMEP: PTFE), where x was 0.5, 1, 1.5, and 2, labeled as Coating-1, Coating-2, Coating-3 and Coating-4, respectively. After magnetic stirring at 500 r/min for 1 h, different contents of dispersion were sprayed on glass substrates for wettability characterization. Finally, the selected dispersion was sprayed on the shape memory composites and cured at 100 °C for 2 h. Before the spraying process, the shape memory epoxy resin was poured into a mold with carbon cloth and pre-cured at 100 °C for 20min.

2.3. Characterization of SSMC

2.3.1. Evaluations on surfaces' properties

Scanning electron microscopy Thermo QuattroS (Czech) was used to investigate and analyze the hierarchical structure of the SSMC. Its surface roughness was then investigated by 3D optical microscopes (Bruker Contour GT-X, Germany). The chemical properties of SSMC were simultaneously evaluated by energy dispersive spectroscopy (EDS, EDAX ELECT PIUS, UK). XPS and FTIR were employed to characterize the surface chemistry, which are Thermo Nexsa and Thermo Nicolet iS5, (USA), respectively. The contact angle meter (Shengding-100 S, China) was employed to evaluate the surface wettability.

2.3.2. Shape-memory behavior characterization

Dynamic thermomechanical analysis (DMA) was employed to investigate the thermo-mechanical properties of the samples between 25 and 200 °C at a heating rate of 3 °C/min and under a strain applied at a constant frequency of 1 Hz. The shape recovery performance of SSMC (10 × 30 mm) was evaluated by shape recovery ratio and recovery time.

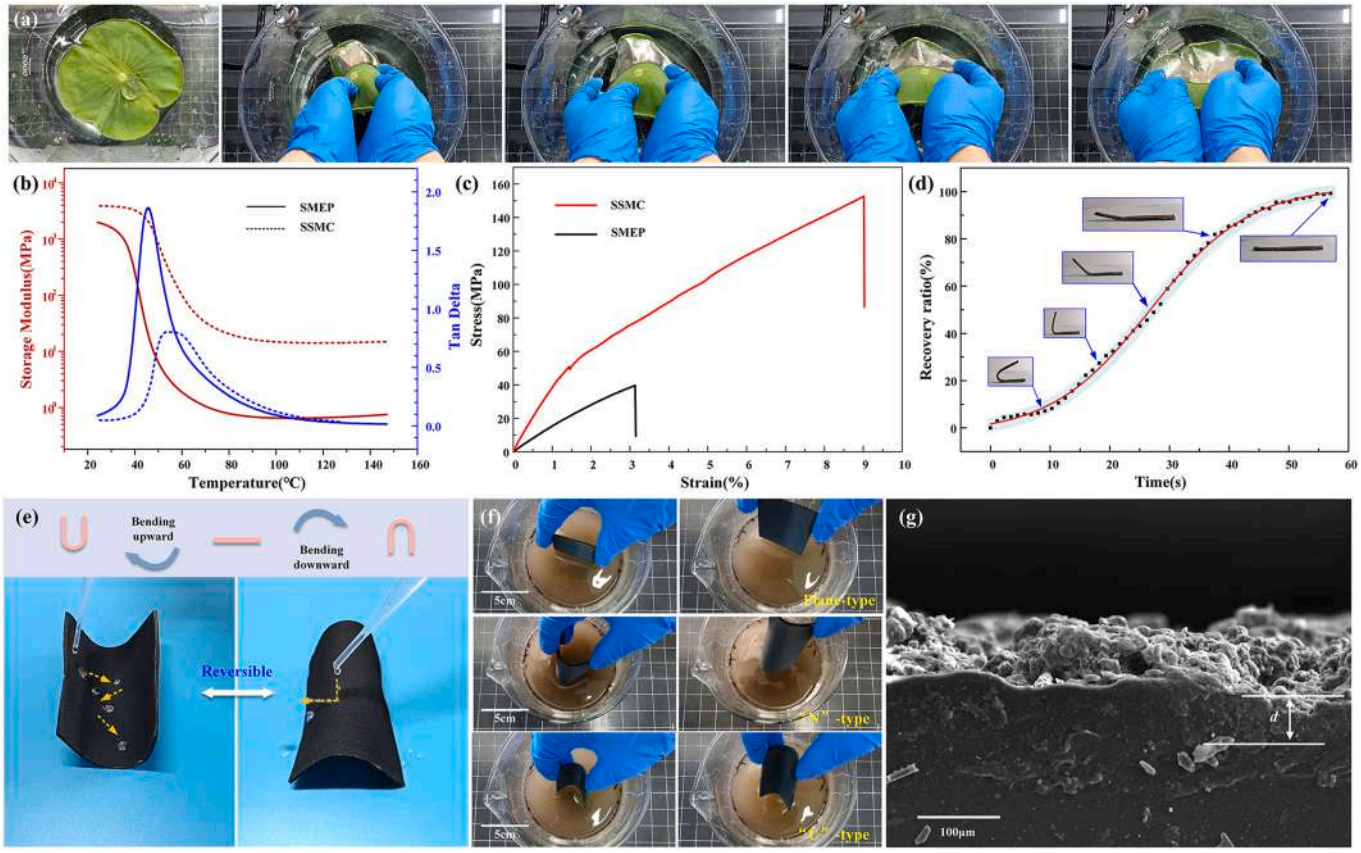

Fig. 3. (a) Sliver mirror performance on Lotus leaf. (b) Dynamic thermomechanical test (DMA) of SMEP and SSMC. (c) Room-temperature mechanical properties of the SMEP and SSMC. (d) Shape recovery ratio of SSMC, and insets are the images of its real-time shape changes. (e) Water repellency of SSMC when bending upward or downward. (f) Self-cleaning performance of SSMC at "Plane-type", "N-type" and "U-type". (g) SEM images of the cross-section of SSMC.

The recovery process was recorded when heating the SSMC with "U" shape above 100 °C and recovering to its original shape.

2.3.3. Anti-icing performance investigation

The anti-icing performance was investigated by a self-made apparatus in the lab, which is sealed to be free from the interference of surrounding environment. When the hermetic temperature reaches 0 °C, water droplets (50 μL) were dropped on the cold samples respectively. And the icing process was recorded and evaluated by freezing delay time and freezing delay temperature.

2.3.4. Drop impact investigation

Water droplets were released through a syringe at different heights of 3 cm, 5 cm, and 7 cm. The diameter of the water droplets was around 3 mm. Due to the shape memory performance of SSMC, the inclination angles were controlled at 15°, 30°, and 45°. And the impact process on SSMC with different inclination angles was recorded by high-speed cameras (Phantom Miro C320, USA) at 2200 fps.

3. Results and discussion

3.1. Surface topography and wettability

The fabrication procedure of the superhydrophobic shape memory composites is illustrated in Fig. 1a. To evaluate the wettability of coatings with different weight ratio of SMEP and PTFE, their water contact angle (WCA) and the water sliding angle (WSA) was investigated, as shown in Fig. 1b. It is found that the Coating-3 (the weight ratio of 1:1.5) provides better superhydrophobicity, where the WCA is 159.3 ± 2° and the WSA is 6.7 ± 1°. Meanwhile, its wettability of different pH droplets was investigated, as shown in Fig. S1. As the pH changed from 2 to 13, WCA and WSA remained constant. However, WCA and WSA were slightly disturbed when the pH reached 1 or 14, indicating that the surface wettability was degraded. From the insets of Fig. S1, it is found that different water droplets such as milk (high protein), coffee (high sugar), and soy sauce (high salt), suspended well on the coatings and exhibited good superhydrophobicity. The "silver mirror effect" was also found on the material under extreme pH conditions, as shown in Fig. S2. Whether the material was placed in strong acid or strong alkaline solutions, it maintained good hydrophobicity due to its chemical stability. Besides, the self-cleaning capacity of the material was tested by covering the surface with sandy soil, and the results are shown in Fig. S3. By imitating the extreme working environments, the sand can be washed from the material surface with liquids of different pH, especially pH1 and pH14. This can be attributed to the low surface tension, which reduces the contact area between material and other impurities. This excellent feature makes it easy to keep the surface clean.

Furthermore, this as-prepared Coating-3 was sprayed on the shape memory polymer composite at the pre-cured state to enhance the interfacial adhesion between the coatings and substrates. The coated shape memory polymer composite also showed good superhydrophobicity with a WCA of 156.3 ± 2° and a WSA of 9 ± 2°. To further investigate the liquid-repellent performance of as-prepared superhydrophobic shape memory polymer composite (SSMC), a water droplet was gradually pressed onto the surface. As shown in Fig. 1c, water droplets can easily detach and move along the coatings without sticking. In addition, a "silver mirror effect" was found on the SSMC surface, indicating that the wetting state is Cassie state (see Fig. 1d).

It is well known that the chemical composition and surface structure are two important factors affecting the surface wettability of materials.

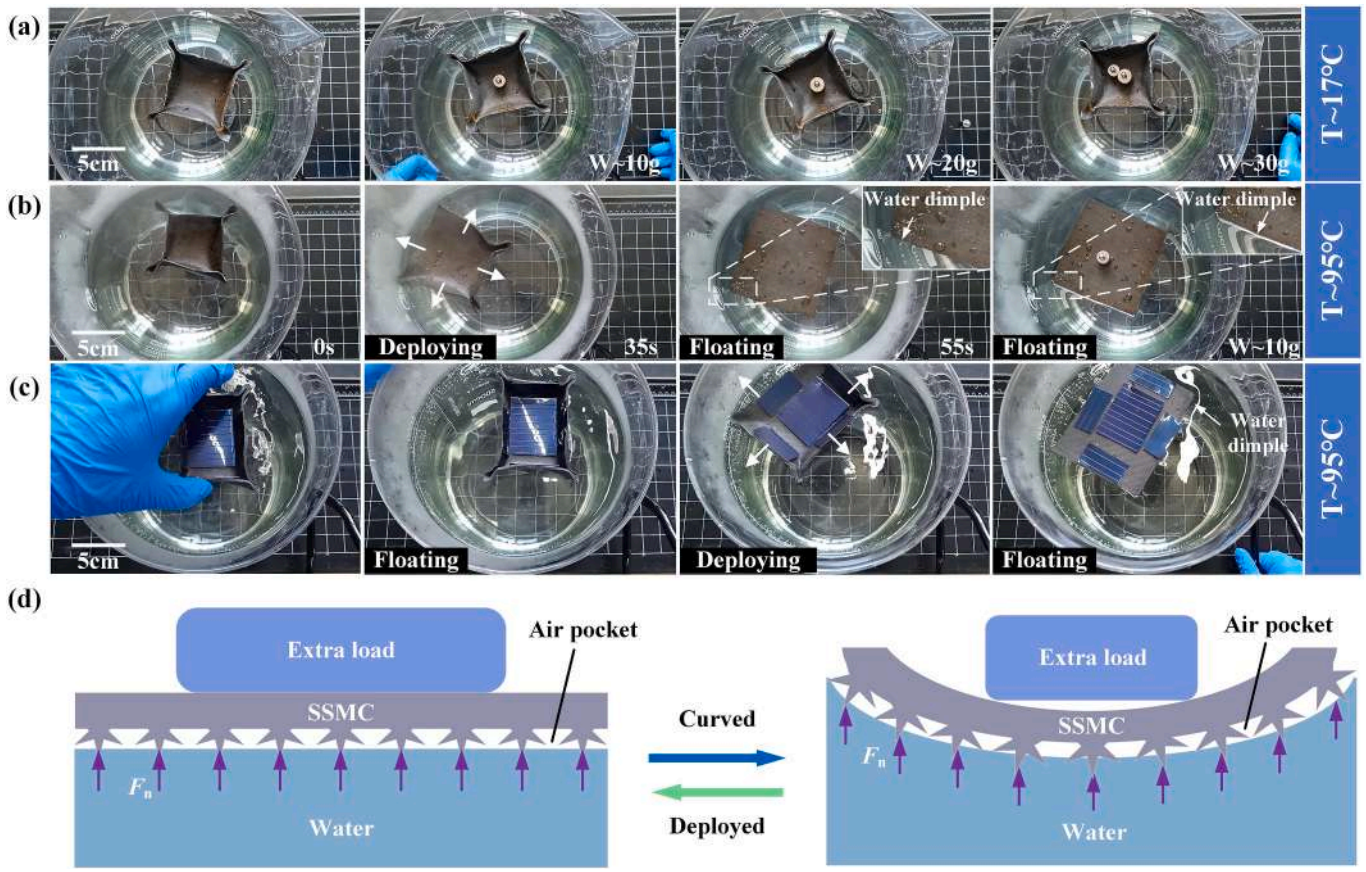

Fig. 4. (a) Origami "boat" by SSMC at 17 °C. (b) Deployable process of SSMC at 95 °C. (c) Demonstration of deployable solar cells by SSMC on the water. (d) Floating mechanism of SSMC at deployed and curved state, respectively.

The surface morphology of the as-prepared superhydrophobic coatings on the glass matrix and shape memory epoxy resin matrix are shown in Fig. 2a–c and d-f, respectively. As shown in Fig. 2a, after the spraying operation, a large number of protrusions were randomly distributed on the surface of the glass substrate, which is similar to the protrusions on lotus leaves. It can also be seen from the enlarged image in Fig. 2b and c that the nanoparticles are densely distributed on the coating surface. When the coating solution was sprayed on the pre-cured shape memory epoxy resin, a rough structure was found on the SSMC but the height of some protrusions was lowered, as shown in Fig. 2d. This should be attributed to the uncured shape memory epoxy resulting in the settlement of protrusions during the final heating process. From the magnification of Fig. 2e and f, it can be seen that many micro-nano particles are also densely distributed on the surface of the coating. To evaluate the surface roughness of the glass substrate coating and SSMC, it was detected by a three-dimensional profile scanner. It can be seen that a large number of irregular bulges and pits are randomly distributed on the surface of the coating in Fig. 2g and h. The Ra of the glass substrate coating and SSMC coating were 13.766 μm and 12.305 μm, respectively.

In addition, XPS, as an effective surface analysis technique, was used to evaluate the chemicals on the as-prepared coating surface on the glass substrate and shape memory composite substrate. From Fig. 2i, it can be seen that the elements of C, O, Si, and F can be detected and evenly distributed on both coating surfaces (see the EDS spectrum in supporting information Fig. S4). From the infrared spectrum of SSMC in Fig. 2j, it can be seen that there are obvious absorption peaks at 2921 cm^{-1}, 1509 cm^{-1}, 1207 cm^{-1}, 1150 cm^{-1}, 887 cm^{-1}, and 487 cm^{-1}, among which the absorption peak at 2921 cm^{-1} is related to the aliphatic C–H of PFOTS [32]. The absorption peaks found in both substrates at 1509 cm^{-1} and 1511 cm^{-1} should be attributed to the C═C stretching vibration of the aromatic structure in the binder [33]. The absorption peaks at 1207 cm^{-1} in SSMC are C-F stretching vibrations in PFOTS and PTFE structures [32], while Si–O bending vibrations are present at 1150 cm^{-1} [34]. Similar absorption peaks were also found on glass substrates. It indicates that the superhydrophobic coatings have been successfully loaded on shape memory composite substrates.

3.2. Characterization of shape memory performance

The lotus leaf is the most popular bionic prototype for its superhydrophobic and self-cleaning properties. From Fig. 3a, it is observed that the flexible lotus leaf exhibits sliver mirror reaction at any bending angle, indicating uniform and stable superhydrophobicity regardless of the folding or unfolding state. From the inspiration, the morphing and wetting performance of the SSMC was further investigated. As shown in Fig. 3a, the dynamic thermomechanical test (DMA) was employed to evaluate the shape memory performance of SSMC. The peak of loss factor (Tan δ) suggests that the glass transition temperature (T_g) of pure SMEP and SSMC is 45 and 56 °C, respectively. It also shows the temperature-dependent storage modulus (E') of pure SMEP and SSMC. At room temperature, the E' of SSMC is 3884 MPa higher than that of pure SMEP. With the increase in temperature, the E' of both samples showed a change in stiffness. And the E' of SSMC (~14.69 MPa) is 20 times higher than that of pure SMEP in the rubber state. Furthermore, the room-temperature mechanical properties of the SMEP and SSMC were measured by Instron testing machine (Instron 3382, USA), and the results are shown in Fig. 3c. From the stress-strain curves, the tensile stress of the SSMC was about 152.7 MPa, three times higher than that of the SMEP (~39.4 MPa). And the elongation of SMEP was also enhanced to 9 % when composited with carbon fabric. The results showed that the SSMC was significantly reinforced by the performance of carbon fabric, which enable it to be potentially applied as industrial deformable

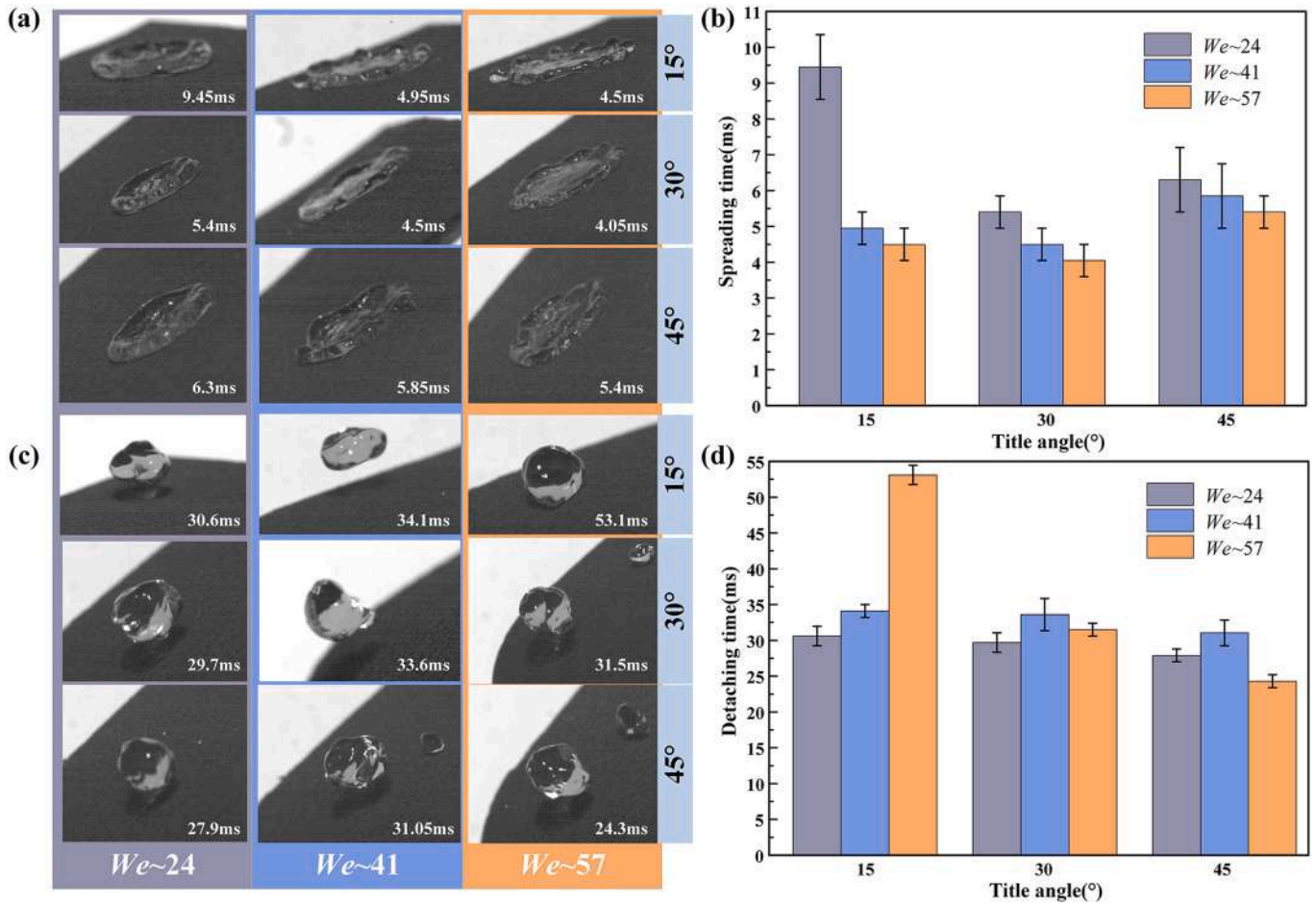

Fig. 5. (a) High-speed images and (c) spreading time of water droplets spreading to the maximum diameters in SSMC at different inclination angles and *We* values. (b) High-speed images and (d) spreading time of water droplets detached from SSMC at different inclination angles and *We* values.

structures. To investigate the shape memory effect of SSMC, the samples were folded into a "U" shape under external loads with temperatures above T_g, and fixed in the folded shape after cooling to ambient temperature. The heat-triggered shape-memory test is employed to characterize the shape recovery ratio in Fig. 3d, and the insets display the real-time shape changes of the SSMC. The original shape was recovered within 57s with a recovery ratio of more than 99 %, indicating its excellent shape memory effect.

In addition, the wettability of SMP-based surface can be altered due to the shape changing of surface topography by pressing, stretching, or bending [35,36]. The surface topography is mostly designed with micro-pillars or micro-lamellae [37,38]. However, it is essential to maintain uniform wetting performance of SSMC at different morphing shapes in diverse situations. As shown in Fig. 3e, the SSMC first bent upward. At this state, the surface structure of SSMC was generally compressed. As the water droplets fell on the curved surface, it was observed that all the water droplets were completely repelled and moved quickly along the surface. When the SSMC was bent downward, the surface structures were under tension. Results showed that water droplets easily bounced off the surface, as dropped on the up-curved SSMC. Thus, the SSMC surface still exhibited non-sticking property. Furthermore, the self-cleaning performance of SSMC was essential when applied in diverse environment. As shown in Fig. 3f, it can be seen that the "Plane-type" SSMC was not contaminated when entering or exiting the muddy water. Interestingly, the SSMC can also protect itself from muddy water like a lotus leaf folded into an “N-type” or “U-type”. It has been proven that the SSMC has good superhydrophobicity regardless of how it is bent, attributed to the good interfacial interaction of the superhydrophobic coatings and SMEP matrix. From the cross-sectional SEM images in Fig. 3g, it is observed that there is no obvious boundary between the superhydrophobic coatings and the shape memory composites, and parts of the regions were merged together. This was further proved by the EDS spectrum. As shown in Figure S5, F and Si elements are embedded in the substrate with the same thickness as characterized by SEM. It is concluded that the as-prepared SSMC can well preserve superhydrophobic, low-adhesion performance even under large scale deformation. The unique water-repellent performance of SSMC enables it to be widely used as morphing skin of aircraft or submarines, especially to maintain the morphing capacity and reduce the drag simultaneously.

3.3. Investigating the potential applications of SSMC

Based on the excellent superhydrophobicity and shape memory property of SSMC, its potential applications in the field of offshore deployable structures were investigated. As shown in Fig. 4a, a quadrilateral structure was fabricated by a simple origami process. To be specific, the SSMC was first heated above the T_g, then folded into a quadrilateral structure. When the temperature dropped below T_g, the unique structure was achieved by removing the external force. It can be seen that the quadrilateral structure well floated on the water (17 °C) even if was loaded with a weight of 30 g. This feature is attributed to its superhydrophobic property which forms a film of air underwater (see Fig. S6) and enhances the buoyancy force. In addition, another fascinating characteristic was the deployment on the hot water. When the quadrilateral structure was placed in 95 °C water, as shown in Fig. 4b, it

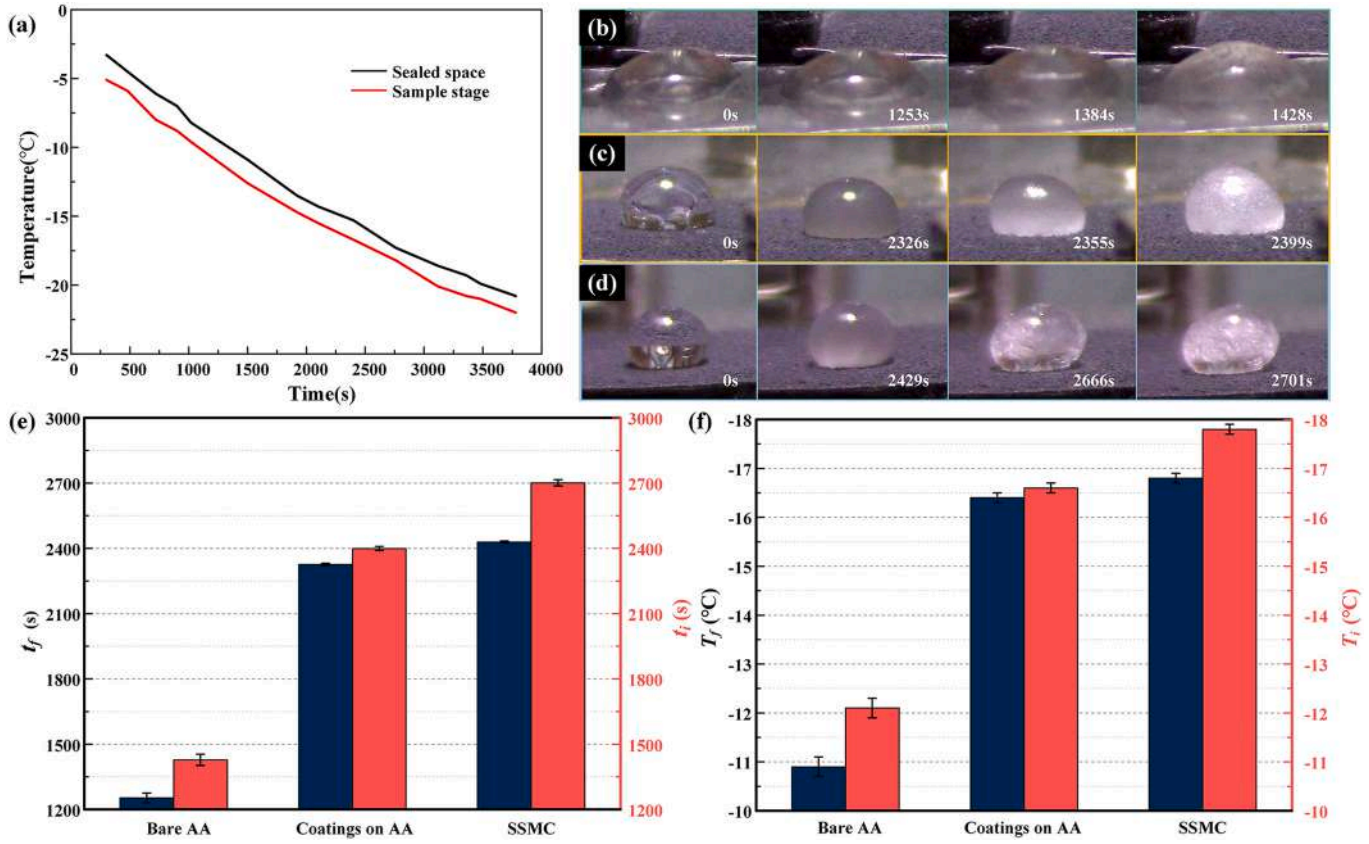

Fig. 6. (a) The cooling rate of the sealed space and the sample stage in self-established apparatus. (b)–(d) Freezing process of water droplets on bare AA, coated AA, and SSMC, respectively. (e) Onset freezing time (t_f) and total ice time (t_i) of SSMC. (f) Onset freezing temperature (T_f) and ice complete temperature (T_i) of SSMC.

automatically returned to its original shape within 55s and floated on the hot water instead of sinking. Subsequently, the SSMC can also bear additional load after being deployed in the soft state. When loaded with another 10 g weight, it can be easily suspended on hot water. As a result, the SSMC can be designed as the deployable floating platform with good folding efficiency and small size collection. Moreover, comparing with the water dimple generated by the surface tension of water, it is more obvious when loaded with extra load, see the insets of Fig. 4b. This floating state of SSMC should be attributed to the supporting force from the curvature and buoyancy forces (F_b) [39,40]. And the buoyancy forces is dominated at this state and proportional to the displacement of water volume. If taken each air pocket as a floating unit, the supporting force of each unit is considered as F_n, as shown in Fig. 4d. Consequently, the total supporting force (F_s) can be written as:

$$F_s \approx F_b \approx \rho(V_0 + abh)g + \sum_1^n F_n \quad (1)$$

where V_0 is the volume of designed structures, ρ and g are the water density and the gravity, a, b and h are the sample's length, and width, and the displacement of water, respectively. According to this formula, it can be concluded that the supporting force of designed structures will be increased by altering its shapes, enlarging the displacement of water volume, and increasing the air pockets. To demonstrate its potential applications for marine deployable structures, the SSMC with quadrilateral structure was utilized to deploy solar cell on the water, as shown in Fig. 4c. It is observed that the folded SSMC-based solar cell gradually deploys and floats on the water eventually. Meanwhile, the superhydrophobic coatings can also act as a functional layer to prevent marine life from attaching. Consequently, the solar cell can be stored in the folded state and deployed at the sea in the working state. It is foreseeable that the SSMC-based solar cells can act as a charging station for marine facilities or unmanned vessels.

In addition, the SSMC can also be designed as a variable-stiffness skin, which is an important part of the morphing wing for aquatic unmanned aerial vehicles (AquaUAV) [41]. Here, we discussed the dynamics of water in morphing wings by investigating the spreading and retraction dynamics of an impacting droplet. It would be a good strategy to spread the water droplets rapidly on the leading edge and detach them from the trailing edge of the morphing wing during the diving process. The impacting process of water droplets on SSMC with different inclination angles experiences preimpact, collision, maximum spread, rebound, detachment, and postimpact stages [42] (see Figs. S7–S9 for details). As seen in Fig. 5a, water droplets spread up to the maximum diameter and showed a pancake shape under a low Weber number (*We*) of ~24 regardless of the inclination angle. And the water droplets quickly spread and appeared as a thin film at *We* ~57. The spreading time of a water droplet is defined as the total time of contact with the surface and spreading to the maximum diameters. From Fig. 5b, it is observed that the spreading time increases with *We*. It was found that the spreading time remained the lowest value at an inclination angle of 30° under different values of *We*. Moreover, water droplets rebounded off the surfaces after complete retraction. As shown in Fig. 5c, the water droplet detached from the surface after 34.1 ms at an inclination angle of 15° and *We* ~41. From Fig. S7, a short "water tail" was found during the detaching process at the inclination angle of 15° and *We* ~57 leading to a longer detaching time. As the inclination angle increased (see Figs. S8 and S9), the "water tail" stretched and the droplets split into two parts with small droplets still in the Cassie–Baxter regime before bouncing off. It indicated that the water droplet penetrated into the air pocket inside the micro-nanostructures, resulting in the wetting transition at the impact site. As seen in Fig. 5d, the detaching time decreased with the increase of the inclination angles regardless of the value of *We*. And the shortest detaching time (24.3 ms) was found at an inclination angle of

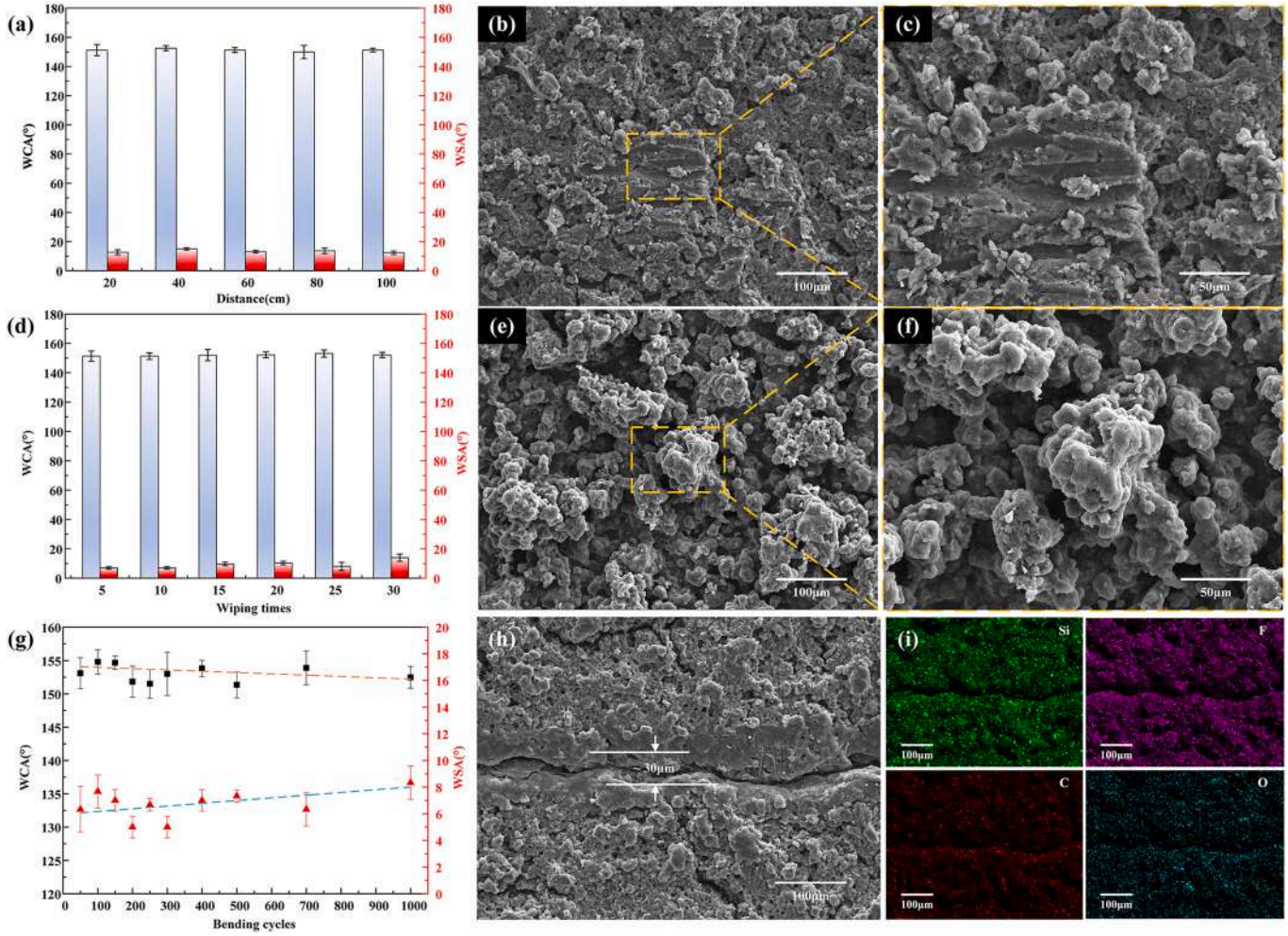

Fig. 7. (a) Wettability of SSMC under sandpaper abrasion. (b)–(c) The SEM images of SSMC after abrasion of 100 cm. (d) Wettability of SSMC under the wiping test of towel paper. (e)–(f) The SEM images of SSMC after 30 wiping times by towel paper. (g) Wettability of SSMC after numerous bending and heating cycles. (h)–(i) The SEM images and corresponding EDS elemental map of SSMC after 1000 times of bending and heating cycles.

45° and $We \sim 57$. As discussed above, the as-prepared SSMC can act as good water-repellent materials for morphing wings in different situations. For the leading edge, the SSMC should be heated and fixed at an inclination angle of 30°, where water droplets reach the maximum diameter in a short time at different velocities. As for the trailing edge, the SSMC presents good water-detaching performance at an inclination angle of 45°. Therefore, the as-prepared SSMC is a good candidate for morphing wing skin of AquaUAV.

To meet the requirements of real applications in winter, it is necessary to investigate the anti-icing performance of SSMC. Freezing delay times and temperatures are often used for evaluation by a self-made device, the cooling rate of which is shown in Fig. 6a. As shown in Fig. 6b–d, water droplets on all tested surfaces exhibited a transparent state during the pre-cooling process, then became non-transparent, and finally changed shape upon be frozen. Consequently, the delayed icing properties were investigated by placing the bare aluminum alloy (AA), coatings on AA, and coatings on SSMC in the sealed capsule of the self-established apparatus when the space temperature decreased to 0 °C. From Fig. 6e, the onset freezing time of a water droplet on SSMC (t_f~2429s) and the total ice time (t_i~2701s) were significantly delayed compared to those of bare AA (t_f ~1253s, t_i~1428s). But the onset time freezing and the total ice time were slightly longer than those of coatings on AA, which were t_f ~2326s and t_i~2399s, respectively. Therefore, the as-prepared SSMC surface presented the best anti-icing performance. Correspondingly, the onset freezing temperature (T_f) of bare AA was −10.9 °C and its total ice temperature (T_i) was −12.1 °C, as shown in Fig. 6f. When covered by superhydrophobic coatings, the T_f and T_i decreased dramatically to −16.4 °C and −16.6 °C, respectively. While for the SSMC surface, the T_f and T_i did not decrease significantly, which were −16.8 °C and −17.8 °C, respectively. It indicates that the as-prepared coatings are useful for inhibiting the freezing process on aluminum alloy and SSMC surfaces. Therefore, the facilities with SSMC can maintain good performance throughout the year.

3.4. Robustness evaluation of SSMC

Robustness is an important property that hinders the application of SSMC. Several methods were selected to evaluate its durability, such as sandpaper polishing, towel wiping, and repeated folding. The abrasion test was performed on 1000# sandpaper to measure the mechanical robustness of SSMC under a certain load of 50 g. As shown in Fig. 7a, as the friction distance increases, the WCA on the surface remains above 150° and the WSA hardly changes. After 100 cm abrasion, the WCA and WSA are 151 ± 2° and 12 ± 1°, respectively, which indicates that the prepared coating has good wear resistance. From Fig. 7b and c, the surface of SSMC still maintains its rough structure after friction, and some friction traces were observed in the local large protrusions. As a result, the hierarchical structures and low surface energy characteristics were well preserved in SSMC. For the friction by soft matters, Fig. 7d demonstrates the relationship between wiping time through paper

towels and wettability of the SSMC surface. Results showed that the WCA of SSMC remained higher than 150°, but the WSA (~14° ± 1°) decreased slightly after wiping for 30 cycles. From the corresponding SEM images in Fig. 7e, the protrusions of the SSMC surface are not obviously damaged. However, the regions above the protrusions were found to be wiped more smoothly, resulting in lower water sliding angles. In addition, the robustness of SSMC after numerous bending and heating cycles should be tested to satisfy the morphing requirements. As shown in Fig. 7g, the WCA of SSMC decreased slowly but remained 152° ± 2° after 1000 times of bending. Meanwhile, the WSA increased to 8 ± 1° and exhibited low adhesion characteristics. From Fig. 7h, a gap of ~30 μm appeared on the SSMC surface after 1000 times of bending, while the resting site still maintained the rough structure without degradation. In addition, it can be seen from the EDS elemental map that C, O, F, Si are uniformly distributed on the surface of SSMC, as shown in Fig. 7i, which indicates that the folding treatment has only slightly affected the surface structure instead of changing the chemical composition. As a result, the SSMC exhibited good mechanical robustness under several harsh treatment, showing high potentials in real applications.

4. Conclusion

In summary, we developed a new type of superhydrophobic shape memory composites by a simple spraying method. The as-prepared SSMC presented good superhydrophobicity with a water contact angle of 156.3 ± 2° and a water sliding angle of 9 ± 2°. Compared with similar coatings on glass substrate, a rough structure was obviously found in SSMC, but the height of some protrusions was slightly reduced for the pre-cured coating method. The SSMC exhibited good shape memory performance with a glass transition temperatures (T_g) of 56 °C, which can return to the original shape within 57s and a recovery ratio of more than 99 %. More importantly, the excellent water repellency and self-cleaning performance remain like a lotus leaf no matter how it is bent. To demonstrate the application, the SSMC was tested as a deployable structure at sea. It can float on water and when folded into a boat shape, it weighs 30 g. Based on its variable stiffness characteristics, the SSMC works well as water-repellent morphing wings, where the leading edge and trailing edge of the airfoil can be deformed to 30° and 45° to reduce drag. Finally, the SSMC also presented good anti-icing property and mechanical/chemical robustness. The total ice time of water droplet on SSMC was delayed about two times than that of bare aluminum alloy. And the SSMC remained good superhydrophobicity after 100 cm abrasion, 30 cycles wiping, and 1000 times bending test. These enabled facilities with SSMC to greatly enhance the year-round service performance. It can be expected that the superhydrophobic shape memory composites with uniform wettability will have great potential applications in the future.

Author statement

Xinlin Li (First Author): Conceptualization, Methodology, Investigation, Writing - Original Draft; Bin Zhan: Investigation, Analysis,; Xueting Wang: Visualization, Investigation; Yan Liu: Resources, Validation; Yanju Liu (Corresponding Author): Conceptualization, Validation, Review & Editing; Jinsong Leng (Corresponding Author): Resources, Supervision, Review & Editing.

Declaration of competing interest

The authors declare that they have no known competing financial interests or personal relationships that could have appeared to influence the work reported in this paper.

Data availability

Data will be made available on request.

Acknowledgement

This work was supported by the following funds: National Natural Science Foundation of China (No. 12102105), China Postdoctoral Science Foundation (No. 2021M690834), and Postdoctoral Science Foundation of Heilongjiang Province (No. LBH-Z21156), and Opening Project of the Key Laboratory of Bionic Engineering (Ministry of Education), Jilin University (No. KF20211003).

Appendix A. Supplementary data

Supplementary data to this article can be found online at https://doi.org/10.1016/j.compscitech.2023.110398.

References

[1] G. Yun, W. Jung, M.S. Oh, G.M. Jang, J. Baek, N.I. Kim, S.G. Im, H. Jung, Springtail-inspired superomniphobic surface with extreme pressure resistance, Sci. Adv. 4 (8) (2018), eaat4978.
[2] D. Wang, Q. Sun, M.J. Hokkanen, C. Zhang, F. Lin, Q. Liu, S. Zhu, T. Zhou, Q. Chang, B. He, Design of robust superhydrophobic surfaces, Nature 582 (7810) (2020) 55–59.
[3] H. Zhang, X. Bu, W. Li, M. Cui, X. Ji, F. Tao, L. Gai, H. Jiang, L. Liu, Z. Wang, A skin-inspired design integrating mechano–chemical–thermal robustness into superhydrophobic coatings, Adv. Mater. 34 (31) (2022), 2203792.
[4] S. Oh, J. Shim, D. Seo, M.J. Shim, S.C. Han, C. Lee, Y. Nam, Organic/inorganic hybrid cerium oxide-based superhydrophobic surface with enhanced weather resistance and self-recovery, Prog Org Coat 170 (2022), 106998.
[5] J. Wei, J. Zhang, X. Cao, J. Huo, X. Huang, J. Zhang, Durable superhydrophobic coatings for prevention of rain attenuation of 5G/weather radomes, Nat. Commun. 14 (1) (2023) 2862, 2862.
[6] Y. Wang, S. Yang, J. Zhang, Z. Chen, B. Zhu, J. Li, S. Liang, Y. Bai, J. Xu, D. Rao, Scalable and switchable CO2-responsive membranes with high wettability for separation of various oil/water systems, Nat. Commun. 14 (1) (2023) 1108.
[7] L. Gui, J. Lin, J. Liu, J. Zuo, Q. Wang, W. Jiang, T. Feng, S. Li, S. Wang, Z. Liu, Difference and association of antibacterial and bacterial anti-adhesive performances between smart Ag/AgCl/TiO2 composite surfaces with switchable wettability, Chem. Eng. J. 431 (2022), 134103.
[8] Y. Yu, W. Cui, L. Song, Q. Liao, K. Ma, S. Zhong, H. Yue, B. Liang, Design of organic-free superhydrophobic TiO2 with ultraviolet stability or ultraviolet-induced switchable wettability, ACS Appl Mater Inter 14 (7) (2022) 9864–9872.
[9] C. Li, J. Yang, W. He, M. Xiong, X. Niu, X. Li, D. Yu, A review on fabrication and application of tunable hybrid micro-nano array surfaces, Adv Mater Interfaces 10 (6) (2023).
[10] Z. Cheng, D. Zhang, X. Luo, H. Lai, Y. Liu, L. Jiang, Superwetting shape memory microstructure: smart wetting control and practical application, Adv. Mater. 33 (6) (2021).
[11] S.M. Curtis, M. Sielenkämper, G. Arivanandhan, D. Dengiz, Z. Li, J. Jetter, L. Hanke, L. Bumke, E. Quandt, S. Wulfinghoff, TiNiHf/SiO2/Si shape memory film composites for bi-directional micro actuation, Int J Smart Nano Mat 13 (2) (2022) 293–314.
[12] S. Yang, Y. He, J. Leng, Shape memory poly (ether ether ketone) s with tunable chain stiffness, mechanical strength and high transition temperatures, Int J Smart Nano Mat 13 (1) (2022) 1–16.
[13] F. Zhang, N. Wen, L. Wang, Y. Bai, J. Leng, Design of 4D printed shape-changing tracheal stent and remote controlling actuation, Int J Smart Nano Mat 12 (4) (2021) 375–389.
[14] A. Lendlein, O.E. Gould, Reprogrammable recovery and actuation behaviour of shape-memory polymers, Nat. Rev. Mater. 4 (2) (2019) 116–133.
[15] T. Sauter, M. Heuchel, K. Kratz, A. Lendlein, Quantifying the shape-memory effect of polymers by cyclic thermomechanical tests, Polym. Rev. 53 (1) (2013) 6–40.
[16] Y. Xia, Y. He, F. Zhang, Y. Liu, J. Leng, A review of shape memory polymers and composites: mechanisms, materials, and applications, Adv. Mater. 33 (6) (2021), 2000713.
[17] Y. Shao, W. Du, Y. Fan, J. Zhao, Z. Zhang, L. Ren, Near-infrared light accurately controllable superhydrophobic surface from water sticking to repelling, Chem. Eng. J. 427 (2022), 131718.
[18] X. Bai, Q. Yang, Y. Fang, J. Yong, Y. Bai, J. Zhang, X. Hou, F. Chen, Anisotropic, adhesion-switchable, and thermal-responsive superhydrophobicity on the femtosecond laser-structured shape-memory polymer for droplet manipulation, Chem. Eng. J. 400 (2020).
[19] Y. Wang, H. Lai, Z. Cheng, H. Zhang, Y. Liu, L. Jiang, Smart superhydrophobic shape memory adhesive surface toward selective capture/release of microdroplets, ACS Appl Mater Inter 11 (11) (2019) 10988–10997.

[20] Y. Li, R. Wang, S. Jiao, H. Lai, Y. Liu, Z. Cheng, Beetle-inspired oil-loaded shape memory micro-arrays with switchable adhesion to both solid and liquid, Chem. Eng. J. 461 (2023), 141927.
[21] Z. Wang, K. Wang, D. Liang, L. Yan, K. Ni, H. Huang, B. Li, Z. Guo, J. Wang, X. Ma, Hybrid magnetic micropillar arrays for programmable actuation, Adv. Mater. 32 (25) (2020), 2001879.
[22] X. Wu, Y. Han, Z. Zhou, X. Zhang, C. Lu, New scalable approach toward shape memory polymer composites via "spring-buckle" microstructure design, ACS Appl Mater Inter 9 (15) (2017) 13657–13665.
[23] D. Zhang, L. Liu, X. Lan, J. Leng, Y. Liu, Synchronous deployed design concept triggered by carbon fibre reinforced shape memory polymer composites, Compos. Struct. 290 (2022), 115513.
[24] D. Zhang, L. Liu, P. Xu, Y. Zhao, Q. Li, X. Lan, X. Zou, Y. Li, Y. He, Y. Liu, Ancient papyrus scroll-inspired self-deployable mechanism based on shape memory polymer composites for Mars explorations, Compos. Struct. 304 (2023), 116391.
[25] X. Lan, L. Liu, C. Pan, F. Li, Z. Liu, G. Hou, J. Sun, W. Dai, L. Wang, H. Yue, Smart solar array consisting of shape-memory releasing mechanisms and deployable hinges, AIAA J. 59 (6) (2021) 2200–2213.
[26] G. Ming, L. Liu, Y. Liu, J. Leng, Space deployable parabolic reflector based on shape memory polymer composites, Compos. Struct. 304 (2023), 116327.
[27] X.B. Gong, L.W. Liu, F. Scarpa, J.S. Leng, Y.J. Liu, Variable stiffness corrugated composite structure with shape memory polymer for morphing skin applications, Smart Mater. Struct. 26 (3) (2017).
[28] K. Gross, L. Weiland, ASME. Flexural testing of shape memory polymers for morphing aircraft applications. proceedings of the ASME international mechanical engineering congress and exposition, PTS A and B: mechanics of solids and structures ASME International Mechanical Engineering Congress and Exposition2008 10 (2007) 299–303.
[29] J.T. Cantrell, P.G. Ifju, Experimental characterization of unimorph shape memory polymer actuators incorporating transverse curvature in the substrate, Exp. Mech. 55 (8) (2015) 1395–1409.
[30] J. Sun, Q.H. Guan, Y.J. Liu, J.S. Leng, Morphing aircraft based on smart materials and structures: a state-of-the-art review, J Intel Mat Syst STR 27 (17) (2016) 2289–2312.
[31] T. Li, J. Sun, J. Leng, Y. Liu, An electrical heating shape memory polymer composite incorporated with conductive elastic fabric, J. Compos. Mater. 56 (11) (2022) 1725–1736.
[32] B. Chen, Z. Dong, Y. Jia, J. Li, M. Zhang, K. Zhang, Sepiolite-based superamphiphobic coating with excellent robustness, chemical stability and self-cleaning performance, PROG ORG COAT 157 (2021), 106297.
[33] Y. Li, X. Shi, W. Bai, S. Zhu, Y. Li, J. Ding, Y. Liu, L. Feng, Robust superhydrophobic materials with outstanding durability fabricated by epoxy adhesive-assisted facile spray method, Colloids Surf. A Physicochem. Eng. Asp. 664 (2023), 131109.
[34] M. Luo, X. Sun, Y. Zheng, X. Cui, W. Ma, S. Han, L. Zhou, X. Wei, Non-fluorinated superhydrophobic film with high transparency for photovoltaic glass covers, Appl. Surf. Sci. 609 (2023), 155299.
[35] C. Chen, H. Yao, S. Guo, Z. Lao, Y. Xu, S. Li, S. Wu, Ultra-Robust joule-heated superhydrophobic smart window: dually-switching droplets adhesion and transparency via in situ electric-actuated reconfigurable shape-memory shutters, Adv. Funct. Mater. 33 (3) (2023), 2210495.
[36] X. Liu, S. Kang, D. Zhang, Y. Li, R. Zhao, C. Wu, Z. Cheng, Q. Tao, Y. Liu, A liquid metal–based shape memory composite with the multi-responsive regulation of solid/liquid adhesion, Adv. Compos. Hybrid Mater. 6 (3) (2023) 124.
[37] G. Constante, I. Apsite, P. Auerbach, S. Aland, D. Schoenfeld, T. Pretsch, P. Milkin, L. Ionov, Smart mechanically tunable surfaces with shape memory behavior and wetting-programmable topography, ACS Appl Mater Inter 14 (17) (2022) 20208–20219.
[38] X. Bai, X. Gou, J. Zhang, J. Liang, L. Yang, S. Wang, X. Hou, F. Chen, A review of smart superwetting surfaces based on shape-memory micro/nanostructures, Small (2023), 2206463.
[39] E. Lepore, M. Giorcelli, C. Saggese, A. Tagliaferro, N. Pugno, Mimicking water striders' legs superhydrophobicity and buoyancy with cabbage leaves and nanotube carpets, J. Mater. Res. 28 (7) (2013) 976–983.
[40] J. Zhao, R. Sun, C. Liu, J. Mo, Application of ZnO/epoxy resin superhydrophobic coating for buoyancy enhancement and drag reduction, Colloids Surf. A Physicochem. Eng. Asp. 651 (2022), 129714.
[41] X. Yang, T. Wang, J. Liang, G. Yao, M. Liu, Survey on the novel hybrid aquatic–aerial amphibious aircraft: aquatic unmanned aerial vehicle (AquaUAV), Prog Aerosp Sci 74 (2015) 131–151.
[42] Y.H. Yeong, J. Burton, E. Loth, I.S. Bayer, Drop impact and rebound dynamics on an inclined superhydrophobic surface, Langmuir 30 (40) (2014) 12027–12038.